



Hprelim-10-131 Submitted to

xxxxx Conference, date, place

Parallel Session

xxxx

Electronic Access: [www-h1.desy.de/h1/www/publications](http://www-h1.desy.de/h1/www/publications)

# Measurement of the Azimuthal Correlation between the Scattered Electron and the most Forward Jet in Deep-Inelastic Scattering at HERA

H1 Collaboration

## Abstract

Deep-inelastic scattering events at low  $Q^2$  with a high transverse momentum jet, produced at small angles with respect to the proton beam, are studied with the H1 experiment at HERA. Differential cross sections and normalised distributions are measured as a function of the azimuthal angle difference  $\Delta\phi$  between the forward jet and the scattered electron. Moreover events with a forward jet and an additional jet, measured in the central region of the laboratory frame, allow to study the  $\Delta\phi$  dependence in a phase space region, where a higher proportion of forward jets from additional gluon emission is expected from models based on BFKL type parton evolution. The measurements are compared to predictions of Monte Carlo generators based on different QCD evolution schemes.

# 1 Introduction

The HERA collider has extended the available kinematic range for deep-inelastic scattering (DIS) to regions of small Bjorken- $x$  ( $x \approx 10^{-5}$ ) at moderate four momentum transfers  $Q^2$  of a few  $\text{GeV}^2$ . This is the region of high parton densities in the proton, dominated by gluons and sea quarks. The large  $\gamma^*p$  centre of mass energy available at small  $x$  gives rise to a large phase space for long parton cascades exchanged between the proton and the photon.

In perturbative QCD multiparton emissions are described only with approximations, and in different regions of  $Q^2$  and  $x$  different QCD-based prescriptions are expected to describe the radiation of partons. At large  $Q^2$  the initial state radiation is described by standard DGLAP evolution equations [1] which at leading order resum  $(\alpha_S \ln Q^2)^n$  terms. In this approach the struck quark originates from a parton cascade ordered in virtuality which is reflected by a strong ordering in transverse momenta  $k_T$  of subsequent gluon emissions. At sufficiently small values of  $x$  the BFKL equation [2] should be applicable. In this approximation the evolution is dominated by large leading  $[\alpha_S \ln(1/x)]^n$  terms which are resummed to all orders. Here the cascade is strongly ordered in fractional longitudinal momenta, while there is no ordering in transverse momentum of the partons along the ladder. Compared to the DGLAP scheme more gluons with sizable transverse momentum are emitted near the proton direction. The CCFM evolution [3] is an attempt to unify these two approaches. It introduces angular ordering of emissions to correctly treat gluon coherence effects, and thus in the limit of asymptotic energies the CCFM evolution equation is almost equivalent to the BFKL approach, while reproducing the DGLAP equations for large  $x$  and high  $Q^2$ .

The dynamics of long parton cascades at small values of  $x$  have been tested at HERA in inclusive measurements, however, the proton structure function  $F_2$  is a too inclusive observable to discriminate between different evolution approximations. Hadronic final states with jets in DIS allow to measure observables sensitive to the kinematic structure of gluon emissions. In particular, properties of energetic jets of high transverse momentum produced close to the proton remnant direction in the laboratory frame, referred to as the forward region, are considered to be especially sensitive to the QCD dynamics at low  $x$  [4]. The selection of forward jets with transverse momentum squared of the order of  $Q^2$  suppresses the contribution of  $k_T$ -ordered cascades with respect to  $k_T$ -unordered processes. In addition, the phase space for BFKL effects is enhanced when the fractional jet energy,  $x_{jet} = E_{jet}/E_p$ , is required to be greater than Bjorken- $x$ . Here  $E_{jet}$  and  $E_p$  are the energies of the jet and the incoming proton respectively.

The angular decorrelation  $\Delta\phi$  in the azimuthal angle between the forward jet and the scattered electron is one of the suggested signatures of BFKL dynamics, which has not been systematically investigated with the HERA data so far. In the Quark Parton Model (QPM) process  $e + q \rightarrow e + q$  the simple two-body kinematics constrains the scattered electron and the forward jet to be produced back-to-back and thus predicts at the parton level  $\Delta\phi = \pi$ . Hadronisation effects may induce some smearing to this parton level prediction. As the rapidity separation between the scattered electron and the forward jet increases one expects decorrelation effects since the phase space for additional gluon emissions opens up. Calculations within the BFKL approach, employing the BFKL kernel to next-to-leading order accuracy (NLO BFKL), show an increase of the azimuthal angle correlation when higher order corrections are included for a fixed value of the rapidity distance  $Y = \ln(x_{jet}/x)$  [5]. At the same time, as expected, the forward jet and the outgoing electron become more decorrelated as the rapidity distance between

60 them grows. Correspondingly, in the fixed-order matrix element calculations for the two- and  
61 three-jet cross section one expects much weaker decorrelaton effects with decreasing  $x$ . [6].

62 This paper presents measurements of the inclusive forward jet cross sections and normalised  
63 distributions as a function of the azimuthal angle difference  $\Delta\phi$  between the most forward jet  
64 and the scattered electron in three bins of the rapidity separation between them. The forward jet  
65 cross section as a function of rapidity distance is also investigated. In addition, measurements  
66 of azimuthal correlations are studied for more exclusive topologies of events with a forward jet  
67 associated with a jet produced in the central region of the laboratory frame.

## 68 2 QCD-based Models

69 The measurements will be compared with predictions of Monte Carlo (MC) programs which  
70 model higher order terms by parton showers in the leading logarithm approximation or by quasi-  
71 classical gluon radiation from colour dipoles. Different MC event generators which adopt vari-  
72 ous QCD approaches to model the parton cascade are used.

73 RAPGAP 3.1 [7] matches first order QCD matrix elements to DGLAP based leading-log  
74 parton showers with strong  $k_T$  ordering. The factorisation and renormalisation scales are set to  
75  $\mu_f^2 = \mu_r^2 = Q^2 + p_T^2$ , where  $p_T$  is the transverse momentum of the two outgoing hard partons.

76 DJANGO 1.4 [8] with ARIADNE includes an implementation of the Colour Dipole Model  
77 (CDM) [9] which has as its basic construct a dipole formed by the struck quark and the proton  
78 remnant. Subsequent parton emissions originate from a chain of independently radiating dipoles  
79 formed by emitted gluons. In this approach transverse momenta of emitted gluons perform  
80 a kind of random walk and in this sense CDM is a BFKL-type program. The DJANGO  
81 predictions are referred to as CDM in the following.

82 CASCADE 2.0.1 [10] uses off-shell QCD matrix elements, supplemented with parton emis-  
83 sions based on the CCFM evolution equation. In this paper two different sets of unintegrated  
84 gluon density are used: set  $A0$  with only singular terms of the gluon splitting function [11] and  
85 set 2 including also non-singular terms [12]. Parametrizations for the unintegrated gluon density  
86 are obtained using the CCFM evolution equation to describe the structure function  $F_2(x, Q^2)$  as  
87 measured at H1 [13] and ZEUS [14].

## 88 3 Experimental Method

### 89 3.1 Event selection

90 The data used for this analysis were collected in the 2000 running periods when positrons and  
91 protons with energies of 27.6 GeV and 920 GeV, respectively, were collided, corresponding to  
92 a centre of mass energy of  $\sqrt{s} = 319$  GeV. The integrated luminosity of the data is  $51.5 \text{ pb}^{-1}$ .

93 DIS events are selected by triggers based on electromagnetic energy deposits in the SPACAL  
 94 calorimeter and the presence of charged particle tracks in the central tracker. The event kine-  
 95 matics are defined by inelasticity  $y$ , virtuality  $Q^2$  and Bjorken- $x$ . They are calculated from the  
 96 4-vectors of the incoming and scattered electron. The data are restricted to the kinematic range  
 97 defined by :

- 98 • the energy of the scattered electron  $E'_e > 10$  GeV
- 99 • the polar angle of the scattered electron  $156^\circ < \theta_e < 175^\circ$
- 100 •  $0.1 < y < 0.7$
- 101 •  $5 < Q^2 < 85$  GeV<sup>2</sup>
- 102 •  $0.0001 < x < 0.004$

103 Jets are identified from combined calorimeter and track objects using the  $k_T$  cluster al-  
 104 gorithm in the longitudinally invariant inclusive mode [15] applied in the Breit frame. The  
 105 reconstructed jets are then boosted to the laboratory frame. The selection further requires the  
 106 reconstruction of at least one forward jet satisfying the following criteria in the laboratory frame:

- 107 • the transverse momentum of the jet  $p_{T,jet} > 6$  GeV
- 108 • the polar angle of the jet  $7^\circ < \theta_{jet} < 20^\circ$
- 109 • the fraction of the proton's energy of the jet  $x_{jet} = E_{jet}/E_p > 0.035$
- 110 •  $0.5 < p_{T,jet}^2/Q^2 < 6$

111 The last condition suppresses the phase space for DGLAP evolution. The upper cut on  $p_{T,jet}^2/Q^2$   
 112 is chosen to reduce migrations in the analysed phase space region, which are related to the  
 113 limited resolution of the  $p_{T,jet}$  measurement. The selection of forward jets with large fractional  
 114 energy  $x_{jet}$ , such that  $x_{jet} \gg x$ , enhances the phase space for BFKL effects. If there is more  
 115 than one jet fulfilling the above requirements, the most forward jet is chosen.

116 Data are presented as differential cross sections as a function of the azimuthal angle dif-  
 117 ference  $\Delta\phi$  between the scattered electron and the most forward jet ( $d\sigma/d\Delta\phi$ ) in bins of the  
 118 rapidity separation  $Y$  between them. The rapidity distance between the scattered electron and  
 119 the forward jet is defined as  $Y = \ln(x_{jet}/x)$ , which corresponds to the evolution parameter in  
 120 the BFKL formalism. For the selected data sample normalised shape distributions  $\frac{1}{\sigma}d\sigma/d\Delta\phi$   
 121 are also determined, where the normalisation is to the total cross section in a given bin of  $Y$ .  
 122 Furthermore, the inclusive forward jet cross section is measured as a function of  $Y$ . Another  
 123 data sample, called "forward jet + central jet" sample, is selected by requiring a forward jet  
 124 satisfying the same selection criteria as above to be accompanied by a jet in the central region  
 125 of the laboratory frame. The additional jet is required to have a transverse momentum above 4  
 126 GeV and to lie in the pseudorapidity region  $-1 < \eta_{jet} < 1$ . These selection criteria provide  
 127 further constraints on the kinematics, control background from radiative QPM-like events and  
 128 reduce effects of soft parton radiation.

## 3.2 Correction procedure and systematic uncertainties

The data are corrected to hadron level using a bin-by-bin correction procedure employing event samples generated with the RAPGAP and DJANGO MC programs and having passed the H1 detector simulation. The correction factors are calculated as the ratio of the CDM model prediction at the non-radiative hadron and radiative detector levels. The uncertainty in the correction factors between the two MC models is included in the systematic error.

For each data point of the measured distributions the uncertainties from different sources are added quadratically. The following sources of systematic uncertainty are considered :

- The model dependence of the bin-by-bin acceptance corrections leads to systematic uncertainties of between 2% and 15% for the forward jet cross section.
- The LAr hadronic energy scale uncertainty of 4% gives rise to an uncertainty of 6% to 12% in the measurements of the forward jet cross section.
- The uncertainty on the electromagnetic energy scale of the SPACAL of 1% results in an uncertainty of the forward jet cross section below 2%.
- The uncertainty on the polar angle measurement of the scattered electron of 1% has negligible effect on the cross section measurements.
- The uncertainty on the determination of the trigger efficiency from the data , using monitor trigger samples, leads to (3 – 5)% uncertainty on the cross section measurements.
- The measurement of the integrated luminosity is accurate within 1.5%.

The model uncertainty gives the largest contribution to the total systematic error. The total uncertainty, consisting of the statistical and systematic uncertainties added quadratically, is estimated to be within (8 – 15)% for the inclusive forward jet cross section and (5 – 15)% for the "forward jet + central jet" cross section.

## 4 Cross Sections

### 4.1 Inclusive forward jet cross sections

The inclusive cross section  $d\sigma/d\Delta\phi$  as a function of the azimuthal angle difference  $\Delta\phi$  between the scattered electron and the most forward jet is shown in figure 1 for three intervals of the rapidity distance  $Y$ :  $2.0 < Y < 3.4$ ,  $3.4 < Y < 4.25$  and  $4.25 < Y < 5.75$ . As expected, at higher values of  $Y$ , corresponding to a lower range in Bjorken- $x$ , the forward jet is more decorrelated from the scattered electron.

The predictions of three QCD-based models with different underlying parton dynamics are compared with the data. Predictions of RAPGAP, which implement DGLAP evolution, fall below the data, particularly at lower values of Bjorken- $x$ . Calculations based on  $k_T$ -factorisation

162 and the CCFM equation, labelled CASCADE, clearly overestimate the measured cross section  
 163 in the two lowest  $Y$  intervals, but are only slightly above the data in the highest  $Y$  interval. Here  
 164 set  $A0$  of the CASCADE program is used. The cross section is described best by the BFKL-  
 165 type MC program, labelled CDM, in which gluon radiation is generated by the Colour Dipole  
 166 Model.

167 The shape of  $\Delta\phi$  distributions,  $\frac{1}{\sigma}d\sigma/d\Delta\phi$ , is compared to different MC predictions in the  
 168 lower part of figure 1, where the normalised ratio  $R$  of MC to data is shown :

169

$$R = \frac{\frac{1}{\sigma^{MC}} \cdot \frac{d\sigma^{MC}}{d\Delta\phi}}{\frac{1}{\sigma^{data}} \cdot \frac{d\sigma^{data}}{d\Delta\phi}}. \quad (1)$$

170 The normalisation of the data points results in  $R = 1$  with statistical and total error bars  
 171 given in percentages.

172 The ratio plots show that in the analysed phase space region the shape of the  $\Delta\phi$  distributions is  
 173 well described by all MC models. This observable alone cannot discriminate between DGLAP  
 174 and BFKL dynamics. In figure 2 it is shown that for the RAPGAP model, with strong ordering  
 175 in transverse momenta of subsequent parton emissions, the shape of the distributions in  $\Delta\phi$  is  
 176 only slightly changed when parton showers are switched off. This may indicate that the forward  
 177 jet originates mainly from one of the two partons of the first order QCD matrix elements. In  
 178 this approach the forward jet satisfying the selection criteria is only rarely initiated by hard  
 179 emissions from the parton shower.

180 Data presented in figure 3 indicate that predictions of the CCFM model are sensitive to the  
 181 choice of unintegrated parton density functions. Set  $A0$  with only singular terms of the gluon  
 182 splitting function and set 2 including also non-singular terms give quite different predictions  
 183 for the differential cross sections in all analysed  $Y$  intervals and for the normalised distribu-  
 184 tions at higher values of Bjorken- $x$ . Set 2 gives a reasonable description of the measured cross  
 185 sections in the two lowest  $Y$  intervals except for the region of large  $\Delta\phi$ , however it fails at  
 186 highest  $Y$ . At lower  $Y$  the shape of the  $\Delta\phi$  distributions is not reproduced by this choice of the  
 187 unintegrated gluon density. In the analysed phase space region set 2 describes the normalised  
 188 distributions well, but only in the highest  $Y$  interval gives a reasonable description of the cross  
 189 section  $d\sigma/\Delta\phi$ . It suggests that HERA data on the azimuthal forward jet correlations, the dif-  
 190 ferential cross sections as well as the normalised distributions, can help in the determination of  
 191 the unintegrated gluon density of the proton based on the CCFM evolution.

192 The inclusive cross section  $d\sigma/dY$  as a function of the rapidity separation  $Y = \ln(x_{jet}/x)$   
 193 between the most forward jet and the scattered electron is shown in figure 4. The CDM model  
 194 gives an excellent description of the data in the whole rapidity distance  $Y$ . The predictions of  
 195 RAPGAP fall below the data everywhere, but approach them as Bjorken- $x$  increases. CAS-  
 196 CADE with set  $A0$  describes the data only in the highest  $Y$  interval. At larger rapidity distance  
 197  $Y$ , corresponding to low values of Bjorken- $x$ , predictions of the MC models, CDM and Cas-  
 198 cade, with parton emissions non-ordered in transverse momentum describe the data well.

## 4.2 Forward jet and central jet cross sections

The differential cross section  $d\sigma/d\Delta\phi$  as a function of the azimuthal angle difference  $\Delta\phi$  between the scattered electron and the most forward jet for events with the forward jet associated with a jet reconstructed in the central region is shown in figure 5. The cross section is measured in two intervals of the rapidity separation  $Y$ :  $2.0 < Y < 4.0$ ,  $4.0 < Y < 5.75$ .

For this topology it is required that both jets satisfy selection criteria as described in section 3.1. The additional central jet is demanded to have a large rapidity separation from the most forward jet,  $\Delta\eta = (\eta_{fwdjet} - \eta_{cenjet}) > 2.0$ . This condition enhances the phase space for additional parton emissions between the two jets. If there is more than one central jet, then the one which is most backward is chosen.

From figure 5 it is observed that at lower  $Y$  the predictions of CDM and RAPGAP describe the cross section reasonably well. At high  $Y$  Cascade (set  $A0$ ) is in best agreement with the data, RAPGAP and CDM predictions are below the measured cross section within two standard deviations. The ratio plots, displayed in the lower part of figure 5, show that the shape of  $\Delta\phi$  distributions is well described by all MC models, in analogy to the more inclusive measurements of the previous chapter.

## 5 Conclusions

Measurements of DIS events at low  $Q^2$  containing a high transverse momentum jet produced in the forward direction are presented. Differential cross sections and normalised distributions are measured as a function of the azimuthal angle difference  $\Delta\phi$  and the rapidity distance  $Y$  between the forward jet and the scattered electron. Investigations of azimuthal correlation are performed in different regions of the rapidity separation between the most forward jet and the outgoing electron, for the inclusive forward jet sample and for events with the forward jet associated with a centrally produced jet. To test the sensitivity of the measured observables to QCD dynamics at low  $x$  the data are compared to QCD models with different parton evolution approaches.

Measurements of the cross sections show that at large rapidity separation between the forward jet and the outgoing electron, corresponding to low values of Bjorken- $x$ , parton emissions non-ordered in transverse momentum are important. QCD models which include such mechanism, like the CCFM model and the BFKL-type CDM model, provide better descriptions of the data. In the analysed phase space region the cross sections  $d\sigma/\Delta\phi$  and  $d\sigma/dY$  are sensitive to small  $x$  effects and can discriminate between different QCD approaches.

The normalised shape distributions in  $\Delta\phi$  (eq. 1) however do not discriminate between different QCD parton dynamics approaches. They are well described by BFKL-type, CCFM or DGLAP models. Monte Carlo investigations within the DGLAP framework indicate that partons from first order QCD matrix elements are tagged as forward jets in the phase space investigated here. Data on the azimuthal forward jet correlations, cross sections as well as shape distributions, can help in determination of the unintegrated gluon density of the proton based on the CCFM evolution.

## 238 References

- 239 [1] V. Gribov and L. Lipatov, Sov. J. Nucl. Phys. **15**, 438 and 675 (1972);  
240 L. Lipatov, Sov. J. Nucl. Phys. **20**, 94 (1975);  
241 G. Altarelli and G. Parisi, Nucl. Phys. **B 126**, 298 (1977);  
242 Y. Dokshitzer, Sov. Phys. JETP **46**, 641 (1977).
- 243 [2] E. Kuraev, L. Lipatov and V. Fadin, Sov. Phys. JETP **44**, 443 (1976);  
244 E. Kuraev, L. Lipatov and V. Fadin, Sov. Phys. JETP **45**, 199 (1977);  
245 Y. Balitsky and L. Lipatov, Sov. J. Nucl. Phys. **28**, 822 (1978).
- 246 [3] M. Ciafaloni, Nucl. Phys. **296**, (1988) 49;  
247 S. Catani, F. Fiorani and G. Marchesini, Phys. Lett. **234**, 339 (1990);  
248 S. Catani, F. Fiorani and G. Marchesini, Nucl. Phys. **336**, 18 (1990).
- 249 [4] A. H. Mueller, Nucl. Phys. B (Proc. Suppl.) **18 C**, 125 (1990).
- 250 [5] A. Sabio Vera and F. Schwennsen, “The Azimuthal Decorrelation of Forward Jets in Deep  
251 Inelastic Scattering”, Phys. Rev. **D 77**, 014001 (2008), [arXiv:0708.0549]
- 252 [6] J. Bartels *et al.*, “Associated Jet Production at HERA”, Phys. Lett. **B 384**, 300 (1996),  
253 [arXiv:hep-ph/9604272].
- 254 [7] H. Jung, Comput. Phys. Commun. **86**, 147 (1995).
- 255 [8] K. Charchula, G. A. Schuler and H. Spiesberger, Comput. Phys. Commun. **81**, 381 (1994).
- 256 [9] L. Lönnblad, Comput. Phys. Commun. **71**, 15 (1992).
- 257 [10] H. Jung, Comput. Phys. Commun. **143**, 100 (2002).
- 258 [11] H. Jung, “Unintegrated parton density functions in CCFM”, April 2004, DIS 2004, Strbske  
259 Pleso, Slovakia, [arXiv:hep-ph/0411287].
- 260 [12] M. Hansson and H. Jung, “The status of CCFM unintegrated gluon densities”, April 2003,  
261 DIS 2003, St. Petersburg, Russia, [arXiv:hep-ph/0309009].
- 262 [13] H1 Collaboration, S. Aid *et al.*, Nucl. Phys. **B 470**, 3 (1996), [arXiv:hep-ex/9603004];  
263 H1 Collaboration, S. Adloff *et al.*, Eur. Phys. J. **C 21**, 33 (2001), [arXiv:hep-ex/0012053].
- 264 [14] ZEUS Collaboration, M. Derrick *et al.*, Z. Phys. **C 72**, 399 (1996),  
265 [arXiv:hep-ex/9607002];  
266 ZEUS Collaboration, S. Chekanov *et al.*, Eur. Phys. J. **C 21**, 443 (2001),  
267 [arXiv:hep-ex/010590].
- 268 [15] S. Catani *et al.*, Nucl. Phys. **B 406**, 187 (1993);  
269 S. Catani, Y. Dokshitzer and B. R. Webber, Phys. Lett. **B 285**, 291 (1992).

## Forward jet azimuthal correlations

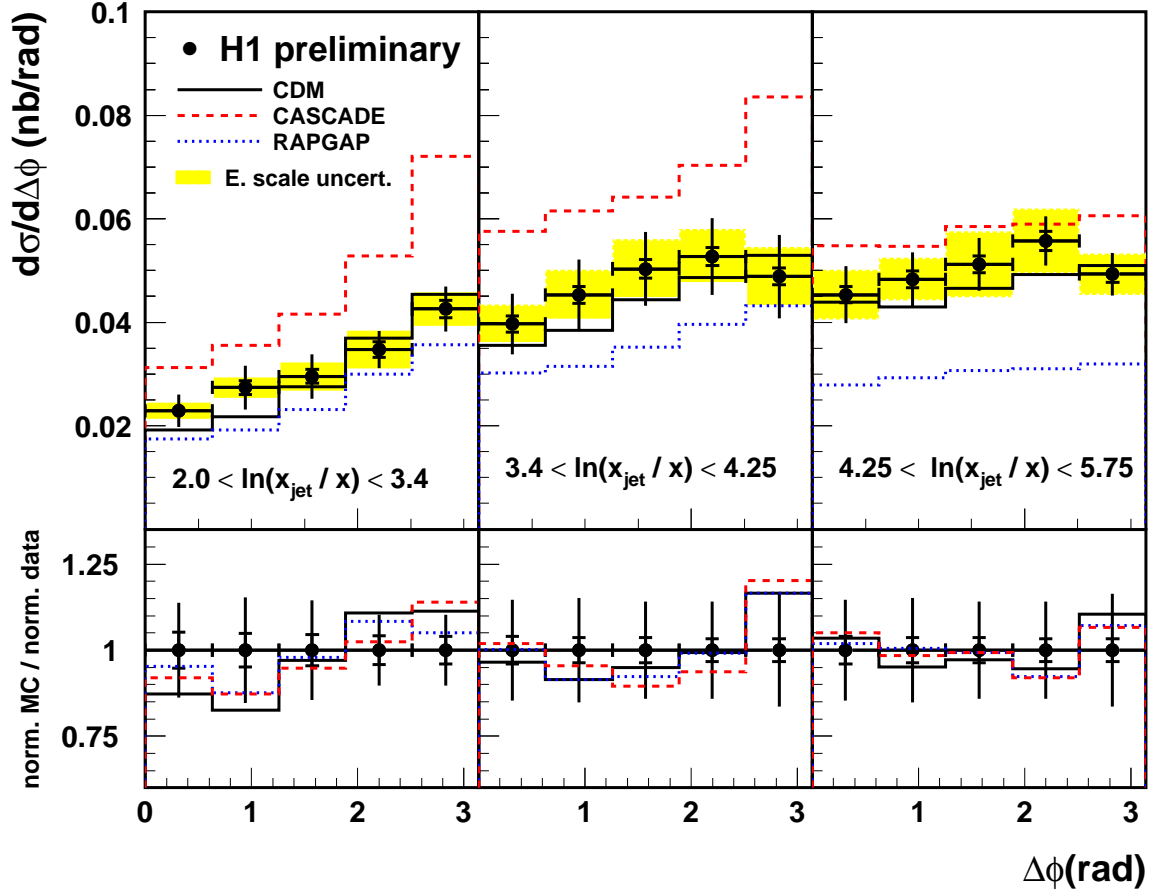


Figure 1: The inclusive forward jet cross section as a function of the azimuthal angle difference  $\Delta\phi$  between the scattered electron and the most forward jet in three intervals of the rapidity distance  $Y = \ln(x_{jet}/x)$ . The inner error bars denote the statistical uncertainties and the outer error bars show the statistical and systematic uncertainties added quadratically. The systematic error due the uncertainty of the hadronic energy scale is shown separately as band around the data points. The predictions of three QCD-based models discussed in the text are shown. In the lower part of the figure the normalised ratio of the theory prediction to data is shown.

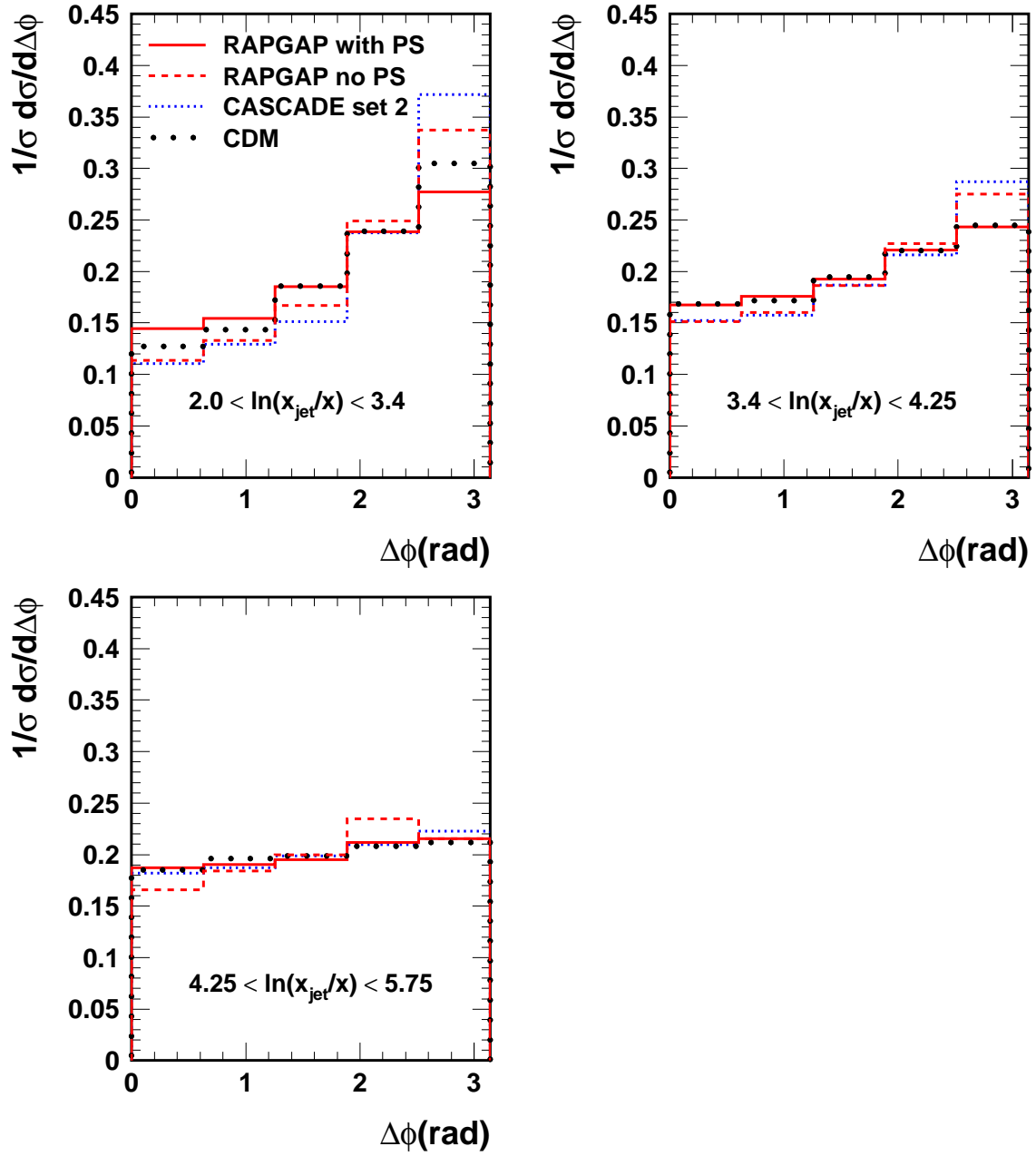


Figure 2: Predictions of the QCD-based model RAPGAP for the normalised forward jet cross section  $\frac{1}{\sigma} \frac{d\sigma}{d\Delta\phi}$  with parton showers on and off.

## Forward jet azimuthal correlations

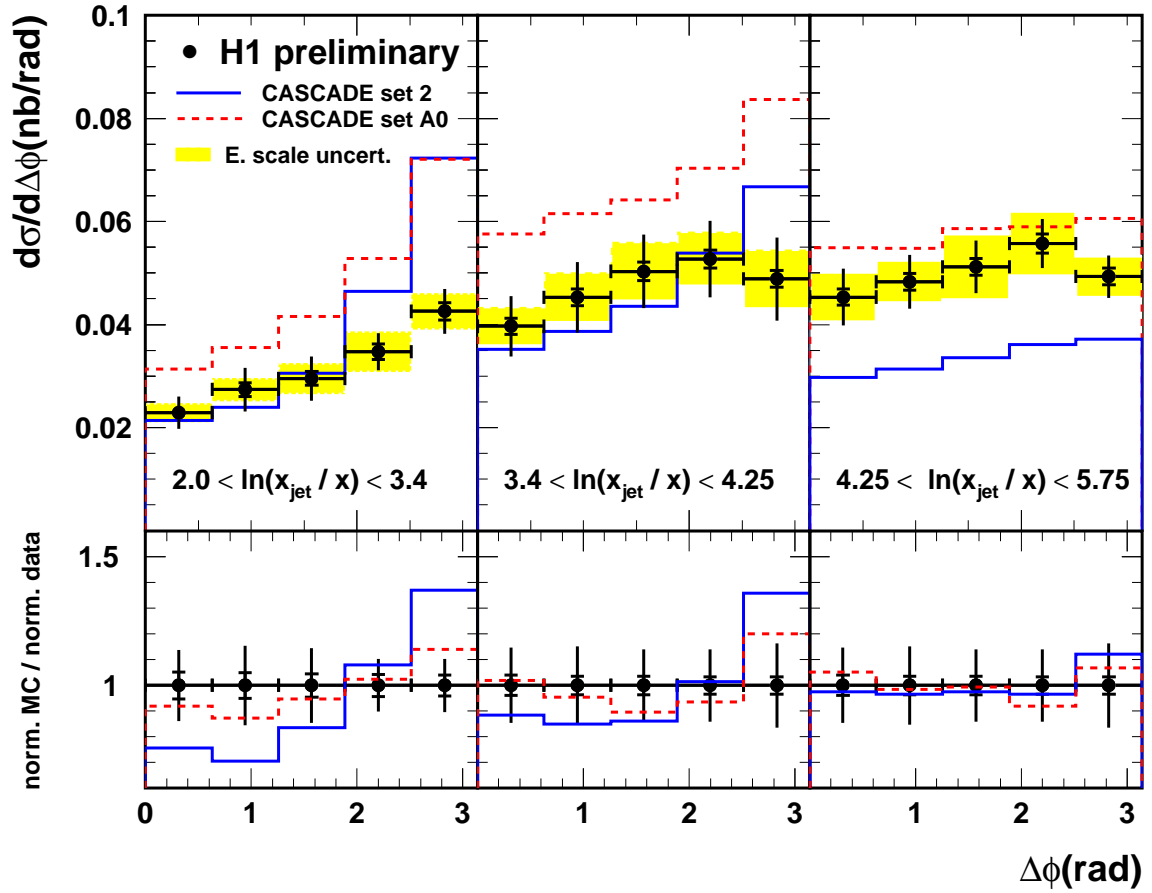


Figure 3: The inclusive forward jet cross section as a function of the azimuthal angle difference  $\Delta\phi$  between the scattered electron and the most forward jet in three intervals of the rapidity distance  $Y = \ln(x_{jet}/x)$ . The data are compared to the predictions of CASCADE with two different sets of unintegrated gluon densities.

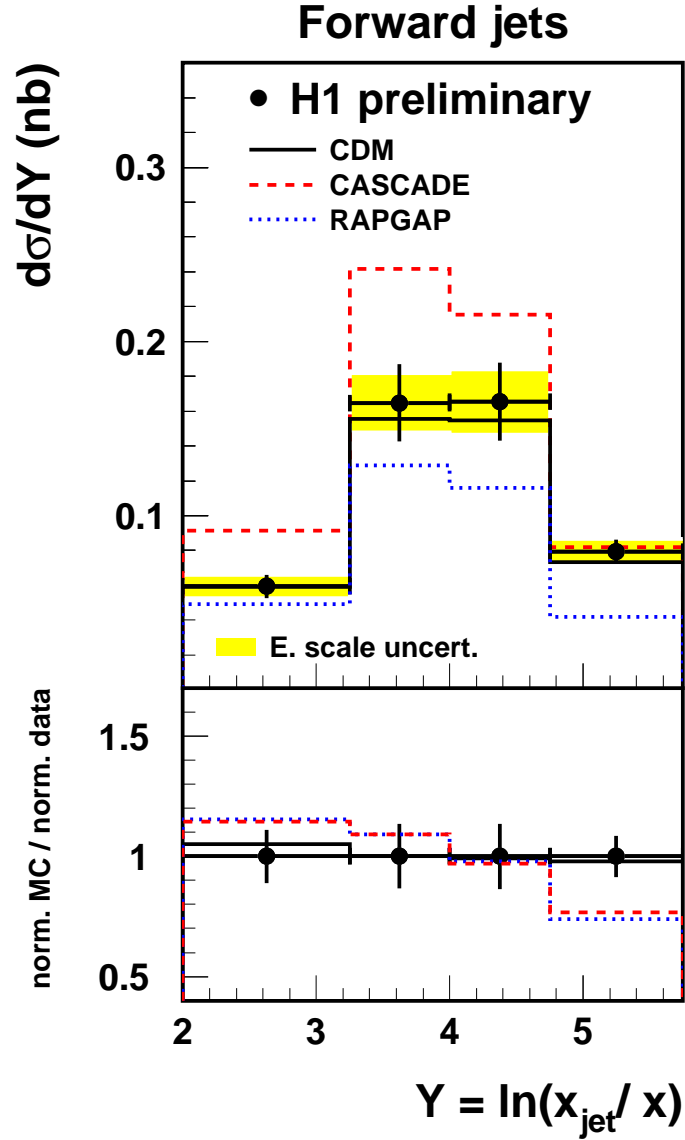


Figure 4: The inclusive forward jet cross section  $d\sigma/dY$  as a function of the rapidity distance between the most forward jet and the scattered electron  $Y = \ln(x_{\text{jet}}/x)$ . The predictions of three QCD-based models discussed in the text are shown. In the lower part of the figure the normalised ratio of the theory prediction to data is shown.

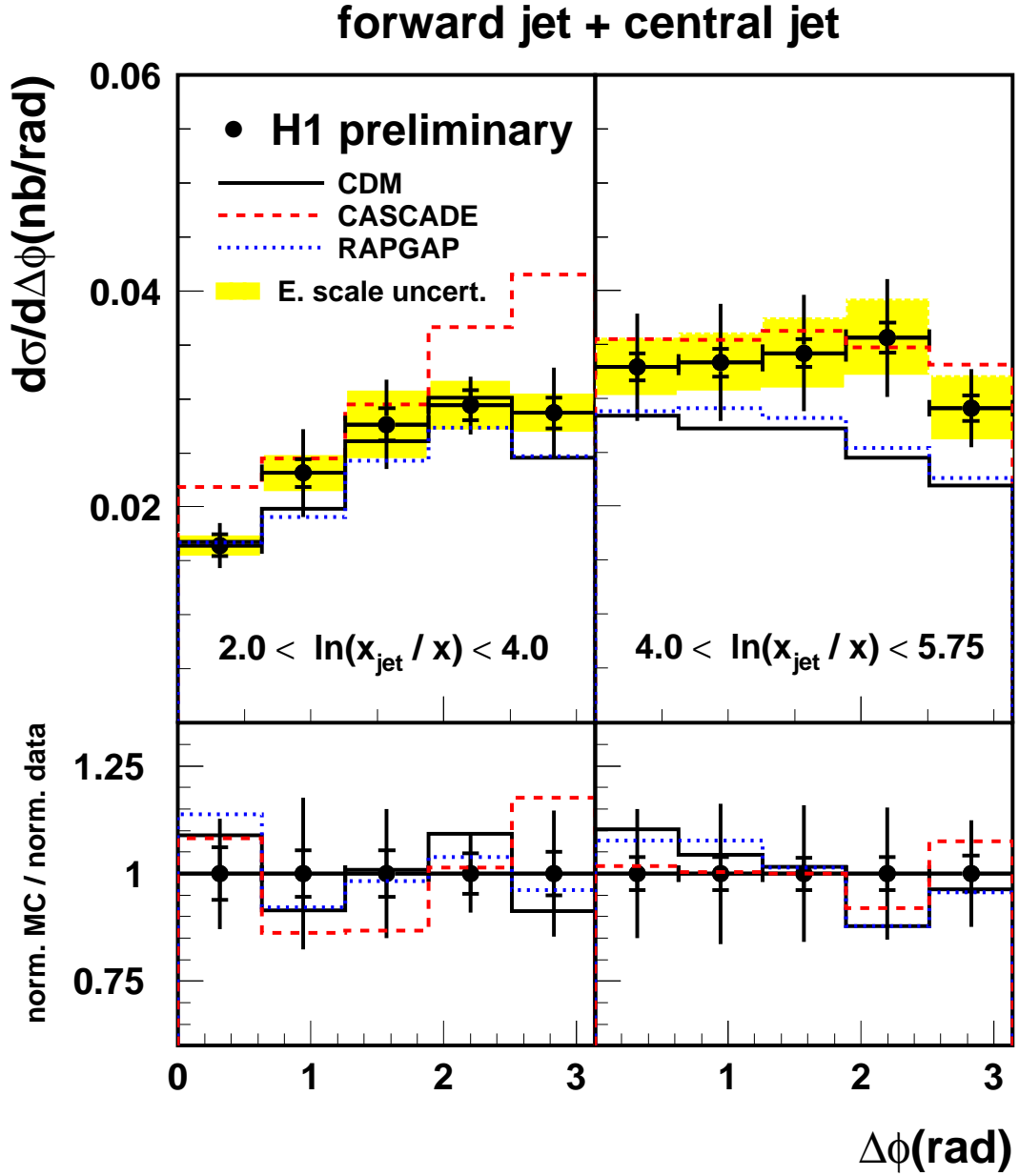


Figure 5: The differential cross section  $d\sigma/d\Delta\phi$  as a function of the azimuthal angle difference  $\Delta\phi$  between the scattered electron and the most forward jet for events with the forward jet associated with a jet reconstructed in the central region. The predictions of three QCD-based models discussed in the text are shown. In the lower part of the figure the normalised ratio of the theory prediction to data is shown.